processes

MDPI

Article

Efficient Preparation and Optimization of Activated Carbon Monoliths from Resorcinol-Formaldehyde Resins for CO_2 Capture

José E. Mosquera [1], Frédéric Delbecq [1], Elias Daouk [1], Audrey Drelich [1], Khashayar Saleh [1], Rémi Gautier [2] and Mikel Leturia [1,*]

[1] Université de Technologie de Compiègne, F-60200 Compiègne, France; euliser87@gmail.com (J.E.M.)
[2] IMT Nord Europe, Institut Mines-Télécom, CERI Energie et Environnement, F-59508 Douai, France; remi.gautier@imt-nord-europe.fr
* Correspondence: mikel.leturia@utc.fr

Abstract: Activated carbon monoliths with developed porosity, high surface area and excellent adsorption properties were successfully prepared from resorcinol-formaldehyde resins using a physical activation method. The primary objective of this study was to examine the impact of key parameters, namely hexamethylenetetramine content (0.08–0.2 g), pyrolysis heating rate (5–20 °C/min) and activation time (1–7 h), on the final characteristics of the activated carbon in order to identify the optimal operating conditions to achieve the desired properties. All the cured resin samples were pyrolyzed at 900 °C under a nitrogen atmosphere, while the activation process took place in the presence of CO_2. The evaluation of the activated carbon materials was based on the CO_2 adsorption capacity and BET surface area, micropore area and total pore volume, which were employed as the criteria for selecting the optimal activated carbon. The synthesized porous carbon monoliths exhibited good properties: high BET surface area (900 m^2/g), high CO_2 adsorption capacity (5.33 mmol/g at 0 °C and 1 bar, 3.8 mmol/g at 25 °C and 1 bar) and good CO_2 selectivity for CO_2/N_2 and CO_2/CH_4 mixtures. These results were obtained with a pyrolysis heating rate of 5 °C/min and a 3 h activation period.

Keywords: resorcinol-formaldehyde resin; porous carbon monolith; physical activation; CO_2 adsorption; CO_2 selectivity

Citation: Mosquera, J.E.; Delbecq, F.; Daouk, E.; Drelich, A.; Saleh, K.; Gautier, R.; Leturia, M. Efficient Preparation and Optimization of Activated Carbon Monoliths from Resorcinol-Formaldehyde Resins for CO_2 Capture. *Processes* **2024**, *12*, 1604. https://doi.org/10.3390/pr12081604

Academic Editor: Monika Wawrzkiewicz

Received: 10 July 2024
Revised: 23 July 2024
Accepted: 24 July 2024
Published: 31 July 2024

1. Introduction

The growing concentration of greenhouse gases in the atmosphere, particularly carbon dioxide (CO_2), has raised significant concerns about global warming and climate change [1]. To address this issue, numerous research studies in the world are actively engaged in the development of efficient sorbent materials for CO_2 capture. Various materials, such as porous carbons, zeolites, porous organic polymers (POPs), metal–organic frameworks (MOFs) and porous silica, are being extensively studied for this purpose [2–4].

Porous carbon-based materials have recently garnered significant attention owing to their competitive advantages, such as high adsorption capacity, large surface area, facile synthesis methods, tunable pore structure, high thermal stability, fast regeneration, low cost and wide availability [5–11]. These materials have also found use in several applications, such as catalysis supports, pollutant removal, energy storage, water and air filtration, as well as natural gas sweetening (CO_2/CH_4 separation) [2,12–14]. Consequently, sorbents based on porous carbons hold great promise in addressing the issue of CO_2 capture.

Over recent years, numerous studies have focused on carbonaceous adsorbents derived from various sources for CO_2 adsorption. These include activated carbons [3,6,15], biomass-derived porous carbons [16,17], metal–carbon composites [18,19], nitrogen-doped carbons [11,12,20–22] and engineered carbon nanomaterials [14,23]. These studies have explored different strategies to enhance CO_2 adsorption capacity, particularly through surface modification, incorporation of heteroatoms (mainly N-containing groups in carbons)

and activation processes. An activated porous carbon (APC) is a solid material with high internal surface area and porosity developed through the carbonization of a precursor and subsequent activation methods, leading to the creation of micro- and mesopores in order to obtain materials capable of adsorbing significant amounts of compounds of diverse chemical natures contained in liquids or gases [24].

Activated carbons are manufactured from carbon-rich raw materials through carbonization (thermal treatment in an inert atmosphere), followed by an activation process, which can be accomplished through chemical activation or physical (or thermal) activation. Chemical activation involves treating the starting material with a concentrated solution of activating agents (KOH, $ZnCl_2$, H_3PO_4, HNO_3, etc.), followed by an exhaustive washing step for chemical contaminants removal. Physical activation is a process by which the carbonized material develops more porosity and a large surface area by eliminating tarry products through heat treatment at temperatures around 800–1000 °C in the presence of oxidizing reactants, such as carbon dioxide, air, steam or mixtures of them [25,26].

In recent years, there has been a growing interest in incorporating nitrogen-containing groups into the framework of activated porous carbons to enhance their CO_2 adsorption capacity and selectivity [5,11,12,20,27–29]. It is believed that the presence of N-functionalities in carbon augments its ability to adsorb CO_2 thanks to the promotion of hydrogen bonding and acid–base interactions between CO_2 molecules with acidic properties and the carbonaceous material [22,30]. However, it should be noted that the impact of N-functionalities on the adsorption performance is not the only factor that needs to be considered. Other factors, such as pore volume and surface area, also play a significant role. For example, Sevilla et al. [31] evaluated the effect of microporous size and N-content on CO_2 adsorption capacity and found that the presence of N-heteroatoms did not have a significant influence on CO_2 adsorption performance.

Various polymeric precursors, such as polyamide, polyetherimide, polyacrylonitrile, poly (acrylonitrile–divinylbenzene), sulfonated poly (styrene–divinylbenzene) and phenolic resins, have been studied for the development of APC by means of pyrolysis [32–36]. Among these, phenolic resins have garnered significant attention as a polymeric precursor due to several advantages, such as easy preparation, very low ash content, low impurities (depending on the synthesis process), relatively low cost, high char yield after carbonization and the ability to be processed into several physical forms, including fibers, spheres, beads, granular structures and even monoliths [35–37]. As depicted in Table 1, several types of activated carbons have been successfully synthesized from phenolic resins, showcasing excellent CO_2 adsorption performance ranging from 1.6 to 8.5 mmol/g at 25 °C and 0 °C.

Table 1. Comparison of CO_2 sorption of different porous carbon materials from the literature.

Author	Morphology	S_{BET} (m^2/g)	CO_2 Sorption Capacity (mmol/g)	
			0 °C, 1 bar	25 °C, 1 bar
Present work	Monolith	908	5.33	3.80
Zhang [36]	Microspheres	1803	-	4.53
Du [8]	Monolith	683	4.01	2.94
Liu [38]	Nanocomposite	442	1.95	1.60
Whang [6]	Nanospheres	1235	7.34	4.83
Wickramaratne [10]	Nanospheres	2930	8.05	4.55
Sevilla [31]	Microspheres	1920	6.25	3.85

To date, most research on the development of CO_2 adsorbents has focused on enhancing certain adsorbent characteristics, including nitrogen functionalities, ordered structures, polymer precursors and activation methods, with the goal of increasing CO_2 adsorption capacity. However, optimizing certain carbonization and activation process variables—such as temperature, inert gas flow, heating rate and time—can also enhance the material's adsorption performance [39]. Consequently, from an engineering standpoint, fine-tuning the parameters related to carbonization and activation conditions can not only enhance

textural and adsorption properties but also result in a reduction in fabrication time. This optimization may also minimize energy consumption, leading to a more sustainable and economically viable overall process.

With these considerations in mind, we propose a scalable and straightforward method for preparing activated carbon monoliths with hierarchical porosities using a resorcinol-formaldehyde resin (RF) obtained through a sol–gel process. The process involves introducing a soft template (Pluronic F127) and hexamethylenetetramine (HMTA) as cross-linking agents and nitrogen sources. The monolith is then solidified at 75 °C, carbonized and thermally activated. The key to this process is the use of HMTA, which decomposes upon heating into ammonia and formaldehyde, aiding in cross-linking and providing a sufficient nitrogen source.

Therefore, the aim of this study is to develop an activated porous carbon monolith from RF resin and enhance its properties, including surface characteristics and adsorption capacity, by optimizing the amount of HMTA, heating rate and activation time. The final goal is to identify the optimal conditions for producing activated carbon monoliths with well-developed porosity and higher yield, following the workflow illustrated in Figure 1. Afterward, the objective is also to characterize the optimal activated carbon material in terms of selectivity, considering the separation of CO_2 from a flue-gas stream on the one hand (CO_2/N_2 separation) and natural gas sweetening on the other hand (CO_2/CH_4 separation). Finally, the adsorption/desorption cyclability of the optimal activated carbon material is characterized.

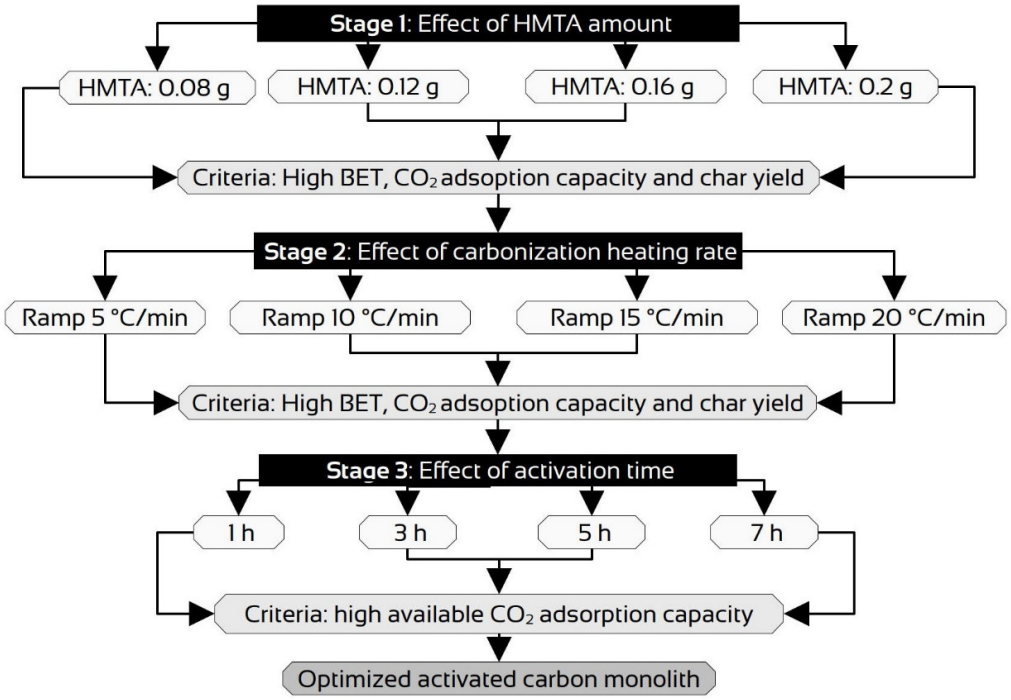

Figure 1. Workflow for the optimization of activated carbon monoliths obtained from RF resins.

2. Materials and Methods

2.1. Materials

Resorcinol (99.0%), hexamethylenetetramine (HMTA, 99.5%), Pluronic F127 and formalin (37 wt % in water) were purchased from Sigma–Aldrich Corp (Saint-Quentin-Fallavier, France). Ethanol (99.9%) was purchased from Carlo Erba reagents (Val-de-Reuil, France). All chemicals were used as received.

2.2. Synthesis of Porous Carbon Monoliths

The resorcinol-formaldehyde resin was synthesized via a sol–gel process, schematically represented in Figure 2, according to the procedure used by Hao et al. [29] with some modifications. In a typical procedure, HMTA (0.57 mmol, 0.08 g) was dissolved in 9 mL of deionized water in a 250 mL flask with magnetic stirring at room temperature. To this solution, ethanol (11.4 mL), Pluronic F127 (1.25 g) and resorcinol (27.3 mmol, 3 g) were added and stirred continuously for 10 min until a homogeneous solution was obtained. The pH of the solution was set around 6.5. Subsequently, formaldehyde (54.5 mmol, 1.63 g) was added quickly to the solution and stirred until the solid was completely dissolved. The resulting clear solution was then transferred to a 25 mL plastic syringe, which was placed vertically in an oven at 75 °C for 24 h. Afterward, the syringe plunger was removed, and the syringe barrel was placed back in the oven at the same temperature for an additional 48 h. The resulting orange polymer monolith was then extracted from the syringe barrel and carbonized in a tubular furnace (24 mm internal diameter) at 900 °C under a nitrogen flow rate of 200 cm^3/min. Thermal activation was carried out using a gas mixture of CO_2/N_2 (20/80 molar%) as the activating agent at the same temperature and flow rate for different activation times, and therefore, different activation progresses. Notably, activation with CO_2 was selected, as it promotes the formation of micropores, which are desirable for CO_2 adsorption operations (compared to H_2O activation, which also promotes less desirable mesopores) [40,41]. Instead of pure CO_2, a gas mixture of CO_2/N_2 (20/80 molar%) was used in the present study to ensure a homogeneous activation in the longitudinal and radial directions of the carbon monolith. The use of this same gas mixture composition is also reported and discussed in the literature [42].

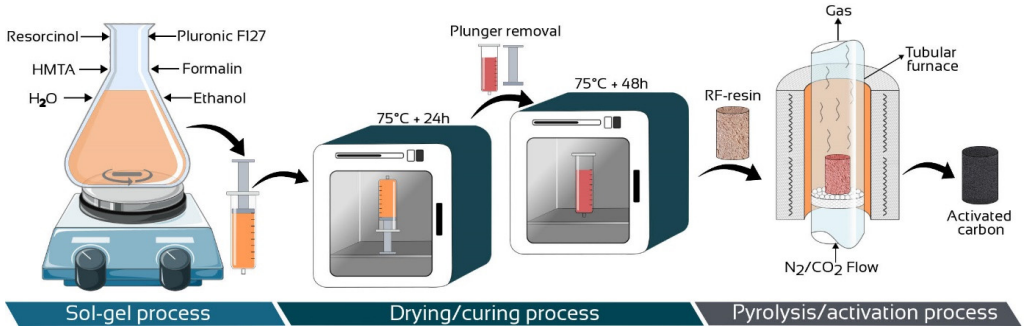

Figure 2. Schematic of the experimental protocol for activated carbon preparation.

2.3. Optimization Procedure

The carbonization process involves the removal of non-carbon components (specifically oxygen, hydrogen and nitrogen) from the precursor materials, resulting in a carbon skeleton with a rudimentary pore structure known as char [25,43]. However, the final characteristics of the activated carbon depend on several experimental parameters, such as carbonization temperature, time, flow rate of inert gas and heating rate [44]. According to Kwiatkowski [39], higher temperatures during carbonization reduce the non-carbon elements in the char and enhance its quality by increasing the surface area and pore volume of the carbon adsorbent. However, this also leads to a reduction in the char yield. During carbonization, the flow of inert gas over the raw material helps prevent carbon burn-off and removes volatile gaseous products from the precursor surface.

For this study, the carbonization temperature (900 °C), hold time (2 h) and inert gas flow rate (200 mL/min) were selected based on preliminary tests and information available in the literature [9,38,45]. Nonetheless, other variables, such as HMTA content, heating rate and activation progress, were found to be more relevant and were consequently evaluated during the optimization process. By carefully considering these factors, it was possible to produce high-quality activated carbon with optimized properties.

For this purpose, the carbon samples obtained at each stage were characterized, and several criteria were considered. The CO_2 adsorption and surface characteristics, including specific surface area, micropore area and pore volume of the produced carbon, were used as primary indicators to select the best conditions. In addition, the char yield and burn-off, after the pyrolysis and activation stages, respectively, were also considered. By evaluating these factors, the aim was to produce an activated carbon monolith with maximum CO_2 adsorption capacity and favorable textural properties, optimal char yield and minimum burn-off. These criteria were essential in establishing the optimal protocol, as they directly impact the performance of the activated carbon materials.

In this study, three parameters were successively investigated to define the optimal experimental conditions and thus obtain the optimal activated carbon, as outlined in Figure 1. Each stage was evaluated based on the established criteria, and the experimental conditions leading to the best performance were selected for the subsequent stage.

- Stage 1: In the first stage, the effect of HMTA on the surface properties and CO_2 adsorption capacity of the resulting material was evaluated. For this purpose, various monoliths were prepared by using different amounts of HMTA (0.08, 0.12, 0.16 and 0.2 g). These monoliths were subsequently carbonized (at 900 °C, 5 °C/min and 2 h) and characterized. The produced carbon materials were labeled as CRF-x, where "x" represents the amount of HMTA added. The amount of HMTA leading to the best porous carbon performance was used for the subsequent stage (according to the above-mentioned criteria).
- Stage 2: In the second stage, the effect of different heating rates (5, 10, 15 and 20 °C/min) during carbonization (900 °C, 2 h) was evaluated. The obtained carbonized materials were designated as CHR-y, where "y" indicates the value of the heating rate employed during carbonization. Again, the carbonization heating rate leading to the best porous carbon performance was used for the subsequent stage.
- Stage 3: Finally, in the third stage, the optimal carbon material obtained from Stage 2 underwent activation for different durations (1, 3, 5 and 7 h). The activated carbons thus produced were denoted as ACR-z, where "z" refers to the applied activation progress. In all these tests, the activation temperature was increased at a heating rate of 20 °C/min under nitrogen until it reached 900 °C. Subsequently, the gas flow was switched from nitrogen to a gas mixture of N_2/CO_2, with a total flow rate of 200 mL/min for the selected activation time. Nitrogen was finally used for cooling down to room temperature.

2.4. Materials' Characterization

Fourier transform infrared (FT-IR) spectra of the RF resins and porous carbons were obtained utilizing a Thermo Scientific Nicolet iS5 with iD1 transmission FT-IR spectrometer (Thermo Scientific®, Waltham, MA, USA) at room temperature in the range of 400–4000 cm^{-1} at a resolution of 4 cm^{-1}, with a KBr pellet. The surface morphology of the samples was analyzed via scanning electron microscopy (SEM) images, with a FEI Quanta 3D FIB FEG instrument (Richland, WA, USA) operated at 20 kV. Elemental analysis was performed on a Thermo Scientific Flash 2000 CHNS/O Analyzer (Thermo Fisher Scientific, Waltham, MA, USA). The textural properties of all activated carbons were determined by N_2 adsorption/desorption at −196 °C using a Micromeritics 3Flex sorption analyzer (Micromeritics, Norcross, GA, USA) with nitrogen of 99.998% purity. Prior to each measurement, all samples were degassed under vacuum at 220 °C for at least 20 h. The specific surface area (S_{BET}) was calculated from the N_2 adsorption isotherm by using the Brunauer–Emmett–Teller (BET) method. Pore size distribution (PSD) was estimated by using the Horvath–Kawazoe (HK) model. The total pore volume (V_{total}), micropore surface area (S_{mic}) and micropore volume (V_{mic}) were calculated using the t-plot method. The CO_2 adsorption capacity of samples was also evaluated using a Micromeritics 3Flex sorption analyzer. Adsorption experiments were conducted at two different temperatures (0 °C and

25 °C) in the pressure range of 0–1 bar. Prior to each adsorption experiment, the samples were degassed at 220 °C for at least 6 h.

2.5. Char Yield, Burn-Off and Available Adsorption Capacity

The char yield refers to the amount of carbon obtained after the carbonization process, expressed as a percentage of the initial mass of the precursor material. It is a measure of the efficiency of the carbonization process and indicates the extent of conversion of the precursor into carbon [46]. The char yield was calculated based on the following equation:

$$Char\ yield\ (\%) = \frac{w_c}{w_0} \times 100 \quad (1)$$

where w_0 (g) and w_c (g) are the initial mass of the precursor and mass of the carbon material after pyrolysis, respectively.

The burn-off determines the activation progress and corresponds to the percentage of mass lost during the activation process of carbon materials [39]. Burn-off is calculated using the following formula:

$$Bo(\%) = Burn - off(\%) = \frac{w_c - w_a}{w_c} \times 100 \quad (2)$$

where w_a (g) is the mass of carbon material after activation.

The activation process leads to a higher surface area but also a higher mass loss of the activated product [25,26]. Thus, determining the optimal balance between CO_2 adsorption performance and the available mass of activated carbon is imperative. For this purpose, the concept of "available CO_2 adsorption capacity", expressed in mmol of CO_2/g of pyrolyzed material, is introduced. This requires the conversion of CO_2 adsorbed per unit mass of activated material (noted as *Ac*) into CO_2 adsorbed per unit mass of pyrolyzed material. The available CO_2 adsorption capacity is calculated as

$$Available\ CO_2\ capacity = Ac\left(1 - \frac{Bo(\%)}{100}\right) \quad (3)$$

where *Ac* (mmol of CO_2/g of activated material) is the CO_2 adsorption capacity of the activated material, and *Bo* is the burn-off (%) during activation.

2.6. Selectivity and Adsorption/Desorption Cyclability of the Optimal Porous Carbon Material

To characterize the selectivity of the optimal activated carbon material (ACR-3), CO_2, N_2 and CH_4 isotherms were measured at 0, 25 and 50 °C, for pressures ranging from 0 to 1 bar using the 3Flex sorption analyzer (Micromeritics, Norcross, GA, USA). Based on these isotherms and using the ideal adsorbed solution theory (IAST) [3,30], the selectivity S_{ads} was estimated using the following equation:

$$S_{ads} = \frac{q_1/q_2}{P_1/P_2} \quad (4)$$

where q_i is the amount of gas *i* adsorbed (mmol/g), and P_i is the partial pressure (bar) of gas *i* in the mixture.

In the present study, the selectivity of the optimal porous carbon material (ACR-3) was estimated considering two typical separation cases:

- Separation of CO_2 from a flue-gas stream, i.e., the separation of a (15:85) CO_2/N_2 mixture;
- Natural gas sweetening, i.e., the separation of a (50:50) CO_2/CH_4 mixture.

Additionally, to assess the cyclability of the optimal activated carbon (ACR-3), 10 consecutive adsorption–desorption cycles were performed on the same sample. In these cycling experiments, the CO_2 adsorption test was conducted at 0 °C and 1 bar, while during the desorption stage, the saturated carbon was heated under vacuum at 130 °C to desorb CO_2.

3. Results and Discussion

3.1. Characterization of the Synthesized Carbon Monoliths

A polymeric resin from HMTA, resorcinol, formaldehyde and Pluronic F127 was successfully synthesized through the sol–gel method. A representative example of an RF resin monolith and its carbonized product are shown in Figure 3a, while Table 2 summarizes the material characterization results. In the photographs in Figure 3a, it is possible to observe that the solid carbon monolith obtained exhibited a uniform shape, similar to that of the RF resin, with a volumetric shrinkage of 55–60% after carbonization (relative to the molds) for all conditions studied. The FT-IR spectrum of the RF resin is presented in Figure 3b. The band at 3425 cm^{-1} was assigned to the N–H and/or OH groups, while the vibrations in the region from 2960 to 2850 cm^{-1} were associated with the C–H bond. Furthermore, the bands observed at 1631 cm^{-1} and 1599 cm^{-1} were assigned to the characteristic absorbance of the aromatic C–H and aromatic C–C stretch, respectively. The band at 1461 cm^{-1} was attributed to CH_2 deformation, and the band observed at 1082 cm^{-1} corresponds to the C–N vibration. Generally, the FT-IR spectrum obtained from the RF resin confirms the presence of characteristic bands typically associated with phenolic resins. These results are also comparable to those obtained by Zhang et al. [36] and Lui et al. [38], who prepared carbonaceous materials from similar phenolic resins. Figure 3b also shows the FT-IR spectrum of the activated carbon (ACR-7), for which several weak bands can be observed. The weak band around 3425 cm^{-1} is attributed to residual N–H and/or OH groups. The weak peaks in the region from 2960 to 2850 cm^{-1} are associated with C–H bonds remaining in the carbon network.

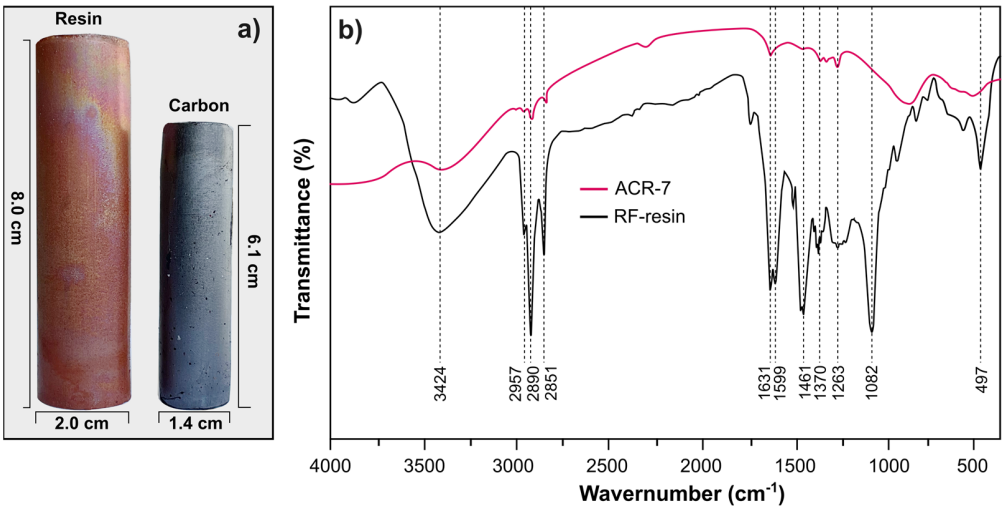

Figure 3. (**a**) Representative photographs and (**b**) FT-IR spectra of as-made resin monolith and activated carbon monolith.

SEM images were employed for the morphological analysis of the carbon materials. Figure 4 displays representative images of the cured resin, as well as carbonized and activated materials. The microspheres in all products exhibited regular and interconnected structures with smooth surfaces. Furthermore, the SEM images also allowed the mean diameter of the individual spheres to be determined (based on 25 measurements). For the RF resin, the particle diameter was measured to be 4.8 ± 0.7 µm, while for both non-activated and activated carbons, the diameter remained similar and close to 2.0 ± 0.6 µm. This reduction in particle diameter suggests that the mass loss during activation primarily resulted from the elimination of residual organic molecules and gaseous products within the bulk of the raw material. Sevilla et al. [31] reported similar observations, where the diameter of resorcinol-formaldehyde-based carbon microspheres remained practically unchanged between non-activated and activated carbons.

Table 2. Adsorption parameters of the porous carbon samples.

Sample	HMTA [a] (g)	Ramp [b] (°C/min)	Activation Time (h)	Char Yield (%)	Burn-Off (%)	N_2 Sorption				CO_2 Sorption (mmol/g)		Elemental Analysis (wt %)			
						S_{BET} [c] (m^2/g)	S_{micro} [d] (m^2/g)	V_{total} [e] (cm^3/g)	V_{mic} [f] (cm^3/g)	0 °C	25 °C	N	C	H	O
CRF-1	0.08	5	-	40.5	NA	353	333	0.18	0.17	3.69		0.53	95.66	0.44	1.40
CRF-2	0.12	5	-	42.3	NA	372	367	0.19	0.19	3.72		0.87	94.74	0.45	1.68
CRF-3	0.16	5	-	42.1	NA	408	382	0.19	0.19	3.76		0.97	94.03	0.42	1.58
CRF-4/CHR-05	0.20	5	-	41.6	NA	450	418	0.21	0.21	4.07	3.17	1.11	94.45	0.42	2.08
CHR-10	0.20	10	-	41.0	NA	412	312	0.21	0.19	3.65		1.00	94.87	0.45	2.04
CHR-15	0.20	15	-	41.6	NA	387	383	0.19	0.19	3.65		1.08	94.44	0.44	2.36
CHR-20	0.20	20	-	41.1	NA	357	330	0.17	0.17	3.62		1.09	95.25	0.46	1.45
ACR-1	0.20	5	1	XX	6	510	473	0.24	0.24	4.62		1.17	92.91	0.42	1.59
ACR-3	0.20	5	3	XX	12	640	600	0.30	0.30	4.99	3.40	1.04	92.85	0.35	1.51
ACR-5	0.20	5	5	XX	16	815	757	0.38	0.38	5.16		1.21	90.27	0.33	1.26
ACR-7	0.20	5	7	XX	22	908	835	0.42	0.42	5.33	3.80	1.19	93.77	0.31	1.16

[a] HMTA content; [b] Heating rate for carbonization; [c] BET specific surface area obtained from the adsorption data in the P/P_0 range from 0.05 to 0.2; [d] Microporous specific surface area obtained using the t-plot method; [e] Total pore volume at a relative pressure of 0.99. [f] Micropore volume. Elemental analysis shown as mean values (n = 3 replicates).

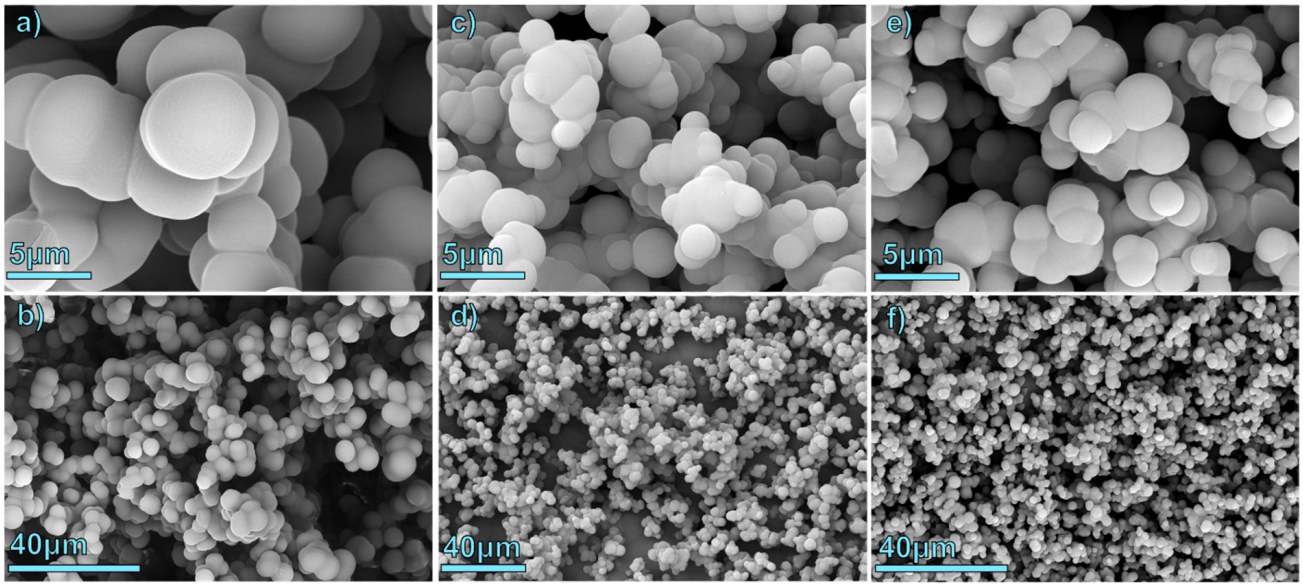

Figure 4. SEM images: (**a**,**b**) RF resin, (**c**,**d**) non-activated carbon and (**e**,**f**) activated carbon.

3.2. Effect of HMTA

In this study, HMTA was utilized as a cross-linker and nitrogen source during the preparation of RF resins [47]. Therefore, the initial focus was to assess the influence of HMTA quantity on the textural properties and CO_2 adsorption performance of the resulting carbon material. To achieve this, a series of RF resins with different amounts of HMTA were synthesized (ranging from 0.08 to 0.2 g) and then carbonized at 900 °C in order to obtain different carbon monoliths. The obtained data are summarized in Table 2 and include textural characteristics, CO_2 adsorption characteristics and elemental analysis.

The elemental analysis revealed an increase in nitrogen content with the addition of HMTA, ranging from 0.53 to 1.11 wt %. This trend was expected, considering that the increase in added HMTA could generate more NH_3 as the principal nitrogen source. Furthermore, the surface characteristics showed a slight increase in the specific surface area (S_{BET}), micropore surface area (S_{mic}) and total pore volume (V_{total}) by increasing the HMTA feed. The highest values of S_{BET}, S_{mic} and V_{total} were all obtained at maximum HMTA content and were equal to 683 m^2/g, 418 m^2/g and 0.23 cm^3/g, respectively. This suggests that HMTA, as a precursor, positively influenced porosity development during carbonization. This finding aligns partially with the observations made by Pajak et al. [9], who found that a certain amount of HMTA used in the initial curing of a cross-linked

Novolac resin had a positive effect on the porosity of the carbonized material (900 °C, 1.5 h, N_2 flow rate of 200 cm^3/min) and the resulting activated product (900 °C, 2.5 h, CO_2 flow rate of 200 cm^3/min). However, the authors also reported that a higher HMTA content in Novolac resin led to an increase in char yield, but excessive cross-linking had a negative influence on porosity. Hence, it is essential to strike a balance between HMTA content and the desired porosity levels.

Furthermore, there is a noticeable increase in CO_2 adsorption capacity of the carbonized material as the HMTA content increases. Among all the samples, CRF-4 exhibited the highest CO_2 uptake of 4.07 mmol/g at 0 °C and 1 bar, which corresponded to improved textural characteristics. The higher HMTA content resulted in a larger surface area, providing more sites for CO_2 adsorption, and also contributed to a higher nitrogen content, which probably further enhanced CO_2 uptake. Importantly, the addition of HMTA did not significantly affect the char yield obtained from the RF resin, which remained almost constant at around 41 wt %. Overall, the increase in HMTA content in the RF resin within the examined range resulted in a higher carbon porosity and enhanced CO_2 adsorption capacity.

However, it should be noted that increasing the HMTA content beyond 0.2 g decreased the mechanical resistance of the resin monolith, making it difficult to remove from the syringe and manipulate without damaging it. Consequently, the maximum HMTA content was set at 0.2 g. Considering the mechanical resistance aspects, as well as surface characteristics and CO_2 adsorption capacity, the CRF-4 sample was selected as the preferred sample for the subsequent stages of the optimization procedure followed in this study.

3.3. Effect of Heating Rate

The heating rate during resin carbonization is an essential factor that significantly impacts both the quality and yield of the final products. In this section, the heating rate was varied within a range of 5 °C/min–20 °C/min to assess its impact on the surface characteristics and adsorption properties of the resulting porous carbons. Table 2 provides an overview of the changes in pore characteristics and CO_2 adsorption capacity associated with the different heating rates.

Interestingly, the char yield remained unaffected by the heating rate, with all samples exhibiting similar values of char yield (~41% wt) and shrinkage (~60% vol). Similarly, elemental analysis indicated no significant influence of the heating rates on the nitrogen content of the chars. In contrast, increasing the heating rate had a negative effect on S_{BET}, S_{mic} and V_{total}. Notably, the best results for pore characteristics were obtained at the lowest heating rate (5 °C/min). Regarding the CO_2 adsorption capacity, the heating rate seemed to have no clear influence between 10 °C/min and 20 °C/min (around 3.65 mmol/g). However, CO_2 adsorption capacity was clearly higher for a heating rate of 5 °C/min (4.07 mmol/g).

Several authors have provided insights into the potential effects of heating rate on the process of carbonization. For instance, Lu and Do [48] have suggested that the heating rate impacts not only pyrolytic reactions but also the rate of particle softening and swelling, thereby affecting the evolution of pore structure. Similarly, Byrne and Nagle [49] have argued that slower heating rates result in a prolonged material dehydration process and may lead to increased cross-linking and cycloaromatization of decomposing polymers, which reduces the production of organic gases and yields a higher char yield. Furthermore, Cetin and coworkers [50] have reported that low heating rates tend to produce a carbon material with a more microporous structure, while high heating rates tend to generate macropores in the carbonized material. According to Tay et al. [51], a lower heating rate is advantageous for pore formation by enabling a gradual release of gases without inducing the collapse or distortion of the char structure. However, it should be noted that a slower heating rate also promotes the shrinkage stage of carbonization, resulting in harder char with reduced pore volume.

Based on these findings, it can be inferred that the impact of heating rate is more significant on pore structure compared to other factors like char yield and shrinkage.

Consequently, reducing the heating rate seems to facilitate the formation of improved porous structures. As a result, the carbon sample (CHR-5) produced at a heating rate of 5 °C/min demonstrated superior CO_2 adsorption capacity and favorable textural properties compared to the higher heating rates evaluated in this work. As a consequence, a heating rate of 5 °C/min was identified as the optimal condition for yielding a porous carbon with the highest S_{BET}, S_{mic} and V_{total}. Therefore, this condition was selected for subsequent experiments in order to evaluate the effects of the other parameters.

3.4. Effect of Activation Progress (Burn-Off)

The carbon materials obtained after carbonization of the resins were physically activated by gasification with CO_2 at 900 °C in order to increase their surface area and enhance the CO_2 adsorption capacity. As expected, the activation progress (burn-off) increased with activation time, ranging from 6% to 22% for activation times of 1–7 h. The effects of the activation progress on pore characteristics and CO_2 adsorption of the activated carbons are depicted in Table 2, as well as Figures 5 and 6.

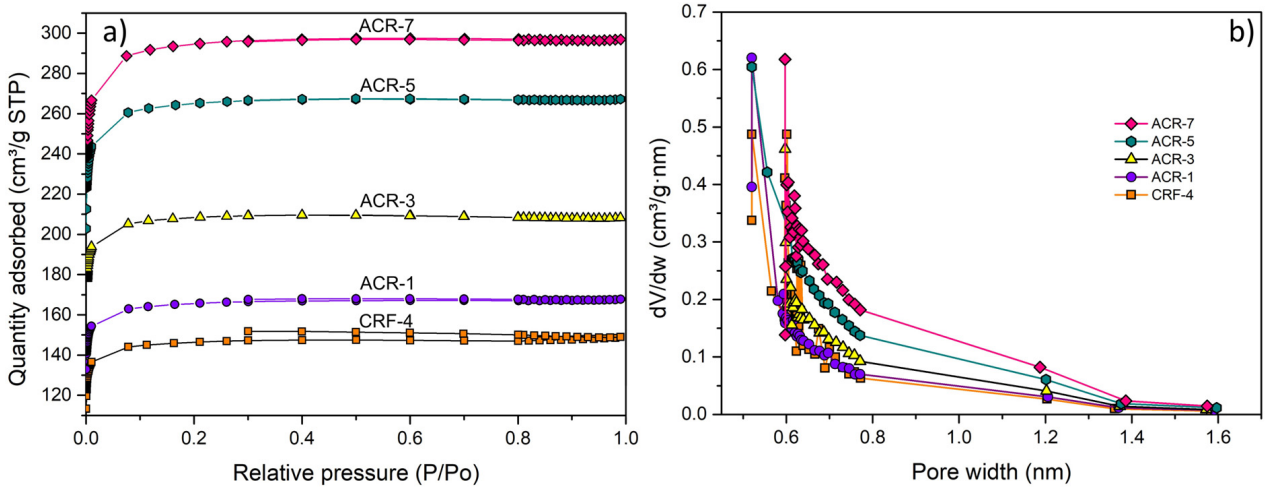

Figure 5. (**a**) Nitrogen sorption isotherms for different activation progresses and (**b**) pore size distributions (PSDs) calculated using the Horvath–Kawazoe method.

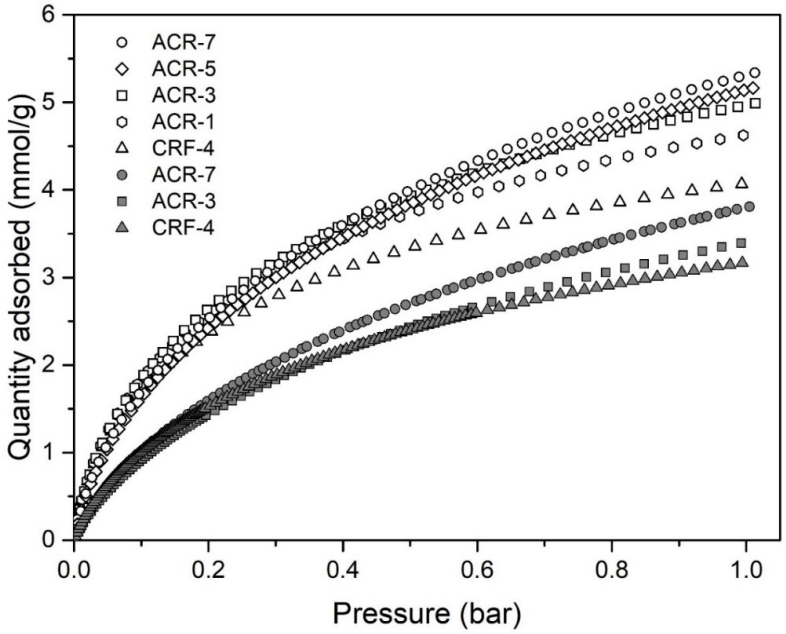

Figure 6. CO_2 adsorption isotherms at 0 °C (open symbols) and 25 °C (filled symbols).

Furthermore, the activated carbon monoliths obtained after the activation treatment did not exhibit any significant physical modifications. Indeed, a very low thermal shrinkage was observed for all the studied conditions (~5% vol). Similarly, there was no clear trend observed in the elemental composition, particularly in terms of nitrogen content.

Regarding the textural characteristics, Figure 5 illustrates the N_2 adsorption isotherms of the activated carbons for different degrees of burn-off and the corresponding pore size distributions. As can be seen, all samples in the study displayed a type I isotherm, indicating the predominant microporous nature of these materials. Type I isotherms are commonly observed in microporous solids, where the filling of micropores takes place predominantly at quite low partial pressures ($P/P_0 < 0.1$) and the adsorption process reaches completion at approximately 0.5 P/P_0 [39,43,52]. Moreover, these isotherms also revealed a small hysteresis loop for non-activated carbon (CRF-4), which then gradually decreased with the subsequent activation, showing that the presence of mesopores was slightly more pronounced in the non-activated carbons compared to the activated samples.

By analyzing the data presented in Table 2, it becomes evident that all samples exhibited a predominance of microporosity, as indicated by the narrow difference between the specific surface area and microporous surface, as well as the close values of the total pore volume and micropore volume. This observation is further supported by the pore size distributions (Figure 5b), which highlighted the prevalence of micropores primarily in the 0.55–0.8 nm range, confirming the predominance of microporous structures in the carbons.

Additionally, it can be observed that the BET surface area, micropore area and total pore volume showed a consistent increase with the activation progress. By varying the activation time from 1 to 7 h, S_{BET} increased from 510 to 908 m^2/g, S_{mic} from 473 to 835 m^2/g and V_{total} from 0.23 to 0.43 cm^3/g. This behavior can be attributed to the extended exposure time, which promotes greater pore development and a higher degree of burn-off, ultimately enhancing the surface properties of the activated carbon. Notably, the activated carbons exhibited significantly higher surface areas compared to the non-activated carbon. Indeed, ACR-7 (7 h activation) demonstrated a surface area of 908 m^2/g, while CRF-4 (no activation) had a surface area of 450 m^2/g, illustrating the improvement in the porous characteristics of the activated material throughout the activation process.

On the other hand, the CO_2 adsorption isotherms measured at 0 °C for the activated carbons are shown in Figure 6. A significant increase in CO_2 uptake was observed between non-activated and activated carbon samples. For instance, the CO_2 adsorption performance of CRF-4 was 4.07 mmol/g, while ACR-7 exhibited 5.33 mmol/g. This remarkable difference highlights the effectiveness of the activation process in enhancing the adsorption properties of the non-activated carbons. These results are in agreement with the improvement observed in textural characteristics, particularly the specific surface area, which exhibited a similar trend. Furthermore, it can be observed that the CO_2 adsorption capacity increased with the activation progress, although the rate of increase was less pronounced at higher activation progress. In addition, it can also be seen in Figure 6 that the resulting activated materials exhibited high adsorption capacities of up to 3.4 mmol/g at 25 °C. This indicates the suitability of the developed material for use in ambient conditions, highlighting its potential for practical applications.

3.5. Production Yields of the Final Products

The primary objective of this study was to identify the optimal process parameters for producing activated carbons with high product yields and maximum adsorption capacity. To achieve this objective, various influential factors, such as HMTA content, heating rate and activation progress, were systematically investigated. As mentioned earlier, when comparing various activated materials, it was evident that both the textural properties and adsorption capacity improved significantly with longer activation time. However, this enhancement came at the expense of increased burn-off, resulting in a reduced amount of effective material at the end of the process. Therefore, it becomes crucial to determine the optimal conditions that yield an activated material with the best balance between

adsorption capacity and the available mass of the activated material. The available CO_2 adsorption capacity, previously defined in Section 2.5 (Equation (3)), allows the conversion of CO_2 adsorbed per unit mass of activated material to CO_2 adsorbed per unit mass of pyrolyzed material. Figure 7 provides a visual representation of the available CO_2 adsorption capacity per unit mass of pyrolyzed carbon as a function of the burn-off degree. Remarkably, the activated product obtained after 3 h of activation (ACR-3) demonstrated the best available CO_2 adsorption capacity, representing the best compromise between adsorption capacity and burn-off (i.e., mass loss of the adsorbent material).

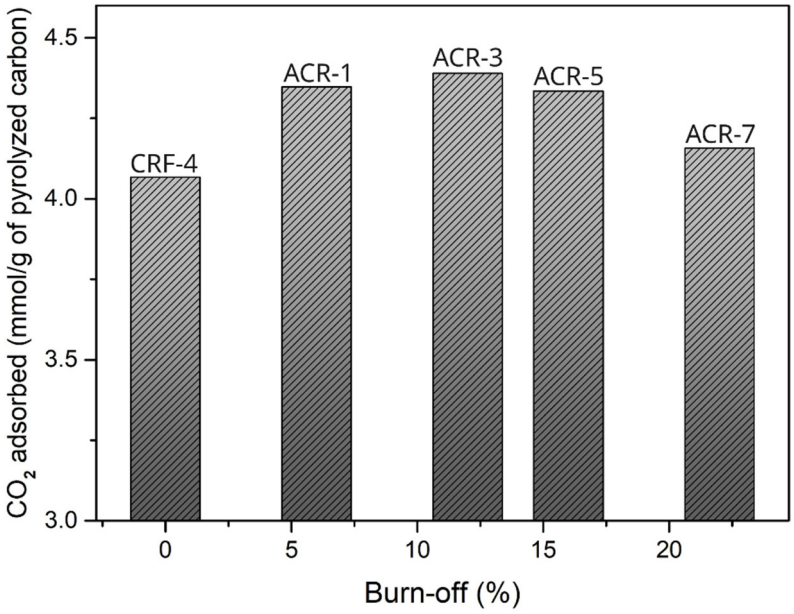

Figure 7. Available CO_2 adsorption capacity of the activated carbons.

Based on these results, the recommended approach for preparing the optimal activated adsorbent is the following:

- The RF resin with a high HMTA content should first be synthesized;
- Carbonization of the cured resin should be carried out at 900 °C, with a heating rate of 5 °C/min;
- Activation progress should be around 12% (corresponding to an activation time of 3 h in the present work).

This carefully selected route ensures the production of an activated adsorbent with superior performance characteristics. In conclusion, by systematically investigating the key parameters and analyzing the resulting data, this study enabled a successful determination of the optimal conditions for producing activated carbons with excellent yield and adsorption capacity. The recommended approach outlined above serves as a practical guideline for achieving desirable outcomes in the production of activated adsorbents from cured resin.

Finally, it should be highlighted that the procedure for fabricating the porous carbon monoliths is simple and easily scalable.

3.6. Selectivity and Adsorption/Desorption Cyclability

As mentioned previously, the obtained activated carbons demonstrated very good CO_2 adsorption capacities. However, further tests were conducted to evaluate the CO_2/N_2 and CO_2/CH_4 selectivities of the optimal activated carbon material (ACR-3), as well as its adsorption stability after several adsorption/desorption cycling runs. All of these results are summarized in Table 3 and depicted in Figures 8 and 9.

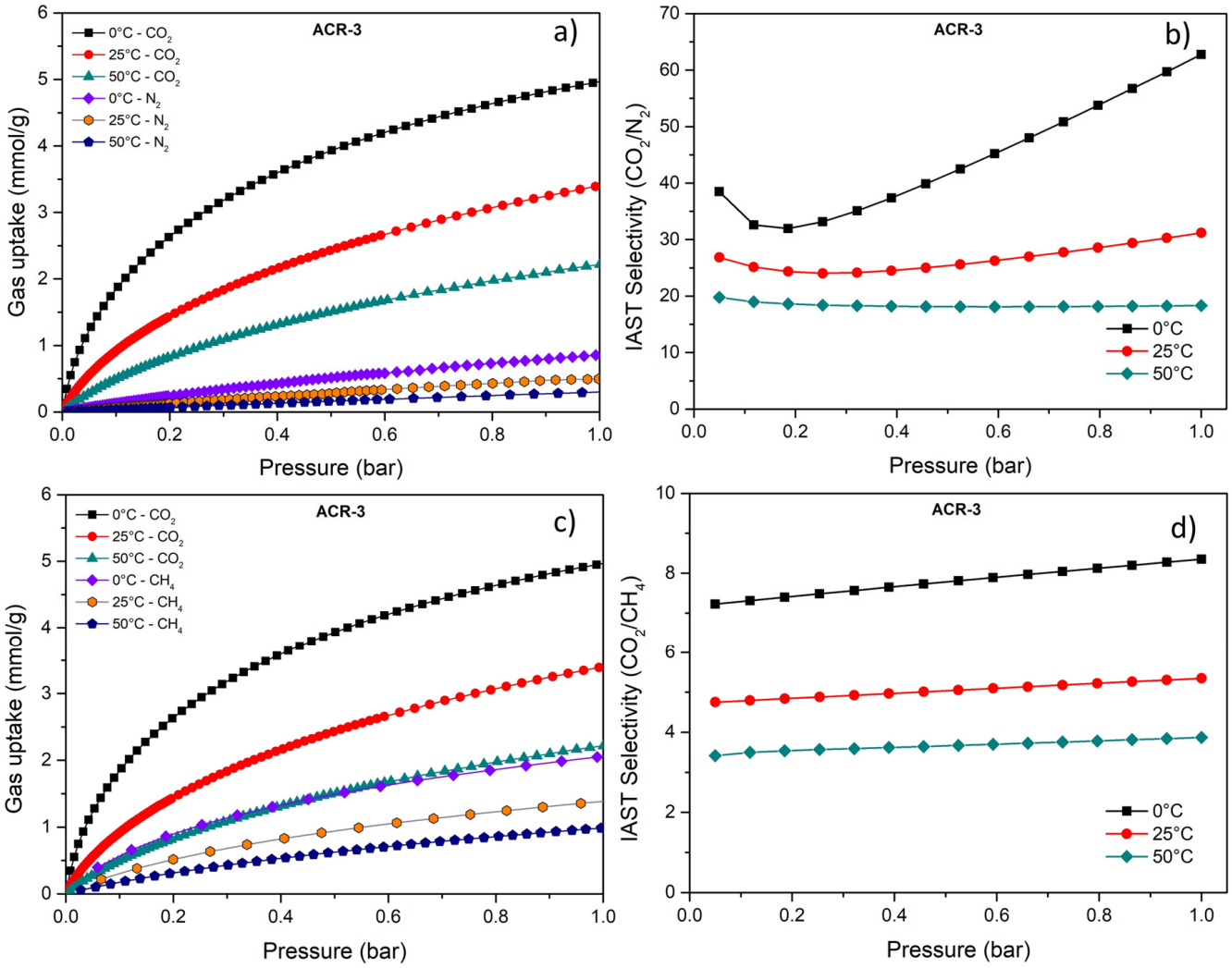

Figure 8. (**a**) CO_2/N_2 adsorption isotherms of ACR-3 at 0 °C, 25 °C and 50 °C, (**b**) IAST selectivity for (15:85) CO_2/N_2 mixture, (**c**) CO_2/CH_4 adsorption isotherms of ACR-3 at 0 °C, 25 °C and 50 °C, and (**d**) IAST selectivity for (50:50) CO_2/CH_4 mixture.

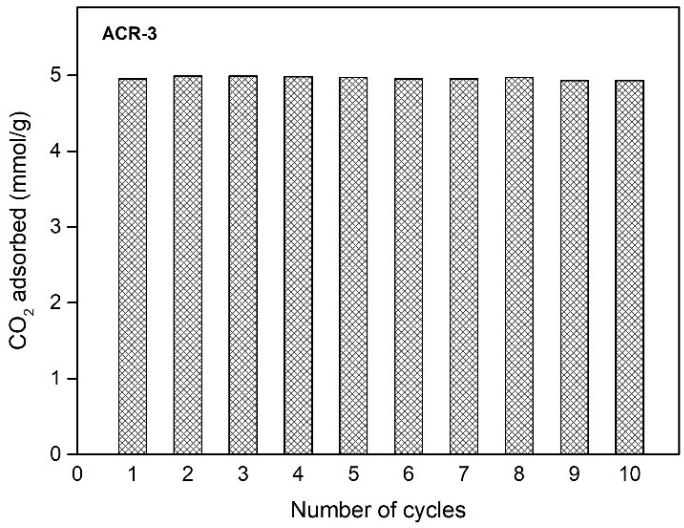

Figure 9. Cyclical CO_2 adsorption behavior of ACR-3: adsorption at 0 °C and 1 bar and desorption under vacuum at 130 °C.

Table 3. Gas uptakes (CO_2, N_2 and CH_4) at 1 bar and IAST selectivity (CO_2/N_2; CO_2/CH_4) for ACR-3.

	CO_2 Uptake at 1 Bar (mmol/g)			**N_2 Uptake at 1 Bar (mmol/g)**			**CH_4 Uptake at 1 Bar (mmol/g)**			**IAST Selectivity CO_2/N_2 (15:85)**			**IAST Selectivity CO_2/CH_4 (50:50)**		
Temperature	0 °C	25 °C	50 °C	0 °C	25 °C	50 °C	0 °C	25 °C	50 °C	0 °C	25 °C	50 °C	0 °C	25 °C	50 °C
ACR-3	4.99	3.39	2.21	0.85	0.50	0.30	2.10	1.40	1.00	62	31	18	8.3	5.3	3.9

As shown in Table 3 and Figure 8a,c, ACR-3 exhibited a higher CO_2 adsorption capacity over N_2 and CH_4 at the different temperatures tested (0 °C, 25 °C and 50 °C). Indeed, at 1 bar, the CO_2 adsorption capacity for ACR-3 ranged from 2.2 to 5 mmol/g, while the adsorption capacity for N_2 and CH_4 only ranged from 0.3 to 0.8 and from 1.0 to 2.1 mmol/g, respectively. As displayed in Table 3 and Figure 8b,d, the IAST selectivity analyses showed that ACR-3 exhibited good performances for CO_2/N_2 separation (separation of CO_2 from a flue-gas stream), as well as for CO_2/CH_4 separation (natural gas sweetening). Indeed, for the CO_2/N_2 (15:85) mixture at 1 bar, the obtained IAST selectivity factors were 62, 31 and 18 at 0 °C, 25 °C and 50 °C, respectively. These values are comparable to those reported in other studies on absorbent carbons [3,6,22,30,53]. The same IAST selectivity analysis was performed for CO_2/CH_4 separation, assuming a 50:50 mixture. At 1 bar, the obtained IAST selectivity factors were 8.3, 5.3 and 3.9 at 0 °C, 25 °C and 50 °C, respectively, which were similar to those reported for PBZ-porous carbon [30] and Zeolite-13X [54].

Regarding the adsorption/desorption cyclability, Wang et al. [55] mentioned that the regeneration for amine-based solid adsorbents is usually carried out between 120 and 170 °C. Therefore, to assess the cyclability of the optimal activated carbon (ACR-3), the adsorption of CO_2 was conducted at 0 °C and 1 bar, while the desorption step was performed under vacuum at 130 °C. Figure 9 displays the evolution of the CO_2 adsorption capacity of ACR-3 at 0 °C and 1 bar during 10 consecutive adsorption–desorption cycles. As can be seen, there was no significant drop in CO_2 adsorption capacity. In fact, the adsorption capacity remained practically constant throughout the runs performed, demonstrating a notable stability. Overall, the high CO_2 adsorption capacity along with good selectivity and excellent stability suggest that the fabricated carbon is a good candidate for CO_2 adsorbent.

4. Conclusions

In this contribution, a novel resin based on resorcinol, formaldehyde and Pluronic F127 as a sacrificial template was synthesized, and its properties were investigated in order to obtain activated carbons with high product yield and maximum adsorption capacity. The study focused on evaluating the influence of key factors, such as HMTA content, heating rate and activation progress, on the resulting carbon material.

Increasing the HMTA content resulted in enhanced porosity development during carbonization, leading to higher specific surface area and total pore volume. These improvements in surface characteristics were directly correlated with an increase in CO_2 adsorption capacity. The heating rate during resin carbonization was also found to play a crucial role in determining the carbon characteristics. Lower heating rates, such as 5 °C/min, promoted the development of a larger surface area and porosity, leading to a superior CO_2 uptake. Regarding the activation process, longer activation times allowed for greater pore development, leading to enhanced surface properties. The activated carbons exhibited substantially higher surface areas and CO_2 adsorption capacities compared to the non-activated carbon. The optimal activation time was determined by finding the best compromise between the increase in adsorption capacity and the mass loss (burn-off), i.e., by identifying the maximum "available CO_2 adsorption capacity".

The recommended approach involves using a RF resin with a high HMTA content, carbonization at 900 °C with a heating rate of 5 °C/min and conducting a 3 h activation process. In addition, it was found that the activated carbon exhibited good selectivity for two typical gas mixtures (CO_2/N_2 and CO_2/CH_4), as well as an excellent adsorption/desorption cyclability, showing its great potential as CO_2 adsorbent.

Author Contributions: Conceptualization, M.L., R.G. and K.S.; methodology, F.D., E.D. and A.D.; validation, J.E.M.; formal analysis, F.D., E.D. and A.D.; investigation, J.E.M.; resources, A.D. and K.S.; data curation, J.E.M.; writing—original draft preparation, J.E.M.; writing—review and editing, M.L., F.D., E.D. and A.D.; visualization, K.S.; supervision, M.L.; project administration, M.L. and R.G.; funding acquisition, M.L. and R.G. All authors have read and agreed to the published version of the manuscript.

Funding: This research was funded by the Région Hauts-de-France (dispositif STIMulE, volet Partenarial) (PISCO Project).

Data Availability Statement: Data will be made available on request.

Conflicts of Interest: The authors declare no conflict of interest.

References

1. Mello, G.; Ferreira Dias, M.; Robaina, M. Wind Farms Life Cycle Assessment Review: CO_2 Emissions and Climate Change. *Energy Rep.* **2020**, *6*, 214–219. [CrossRef]
2. Sai Bhargava Reddy, M.; Ponnamma, D.; Sadasivuni, K.K.; Kumar, B.; Abdullah, A.M. Carbon Dioxide Adsorption Based on Porous Materials. *RSC Adv.* **2021**, *11*, 12658–12681. [CrossRef] [PubMed]
3. Ma, X.; Li, Y.; Cao, M.; Hu, C. A Novel Activating Strategy to Achieve Highly Porous Carbon Monoliths for CO_2 Capture. *J. Mater. Chem. A* **2014**, *2*, 4819–4826. [CrossRef]
4. Lee, J.; Kim, J.; Hyeon, T. Recent Progress in the Synthesis of Porous Carbon Materials. *Adv. Mater.* **2006**, *18*, 2073–2094. [CrossRef]
5. Hao, G.P.; Li, W.C.; Wang, S.; Wang, G.H.; Qi, L.; Lu, A.H. Lysine-Assisted Rapid Synthesis of Crack-Free Hierarchical Carbon Monoliths with a Hexagonal Array of Mesopores. *Carbon* **2011**, *49*, 3762–3772. [CrossRef]
6. Wang, X.; Zhou, J.; Xing, W.; Liu, B.; Zhang, J.; Lin, H.; Cui, H.; Zhuo, S. Resorcinol–Formaldehyde Resin-Based Porous Carbon Spheres with High CO_2 Capture Capacities. *J. Energy Chem.* **2017**, *26*, 1007–1013. [CrossRef]
7. Yang, J.B.; Ling, L.C.; Liu, L.; Kang, F.Y.; Huang, Z.H.; Wu, H. Preparation and Properties of Phenolic Resin-Based Activated Carbon Spheres with Controlled Pore Size Distribution. *Carbon* **2002**, *40*, 911–916. [CrossRef]
8. Du, J.; Li, W.C.; Ren, Z.X.; Guo, L.P.; Lu, A.H. Synthesis of Mechanically Robust Porous Carbon Monoliths for CO_2 Adsorption and Separation. *J. Energy Chem.* **2020**, *42*, 56–61. [CrossRef]
9. Pajak, J.; Labojko, G.; Lachowski, A. Activated Carbons from Crosslinked Novolac Resin. *Adsorpt. Sci. Technol.* **2005**, *23*, 381–386. [CrossRef]
10. Wickramaratne, N.P.; Jaroniec, M. Activated Carbon Spheres for CO_2 Adsorption. *ACS Appl. Mater. Interfaces* **2013**, *5*, 1849–1855. [CrossRef]
11. Nandi, M.; Okada, K.; Dutta, A.; Bhaumik, A.; Maruyama, J.; Derks, D.; Uyama, H. Unprecedented CO_2 Uptake over Highly Porous N-Doped Activated Carbon Monoliths Prepared by Physical Activation. *Chem. Commun.* **2012**, *48*, 10283–10285. [CrossRef] [PubMed]
12. Manmuanpom, N.; Thubsuang, U.; Dubas, S.T.; Wongkasemjit, S.; Chaisuwan, T. Enhanced CO_2 Capturing over Ultra-Microporous Carbon with Nitrogen-Active Species Prepared Using One-Step Carbonization of Polybenzoxazine for a Sustainable Environment. *J. Environ. Manag.* **2018**, *223*, 779–786. [CrossRef] [PubMed]
13. Yu, J.; Guo, M.; Muhammad, F.; Wang, A.; Zhang, F.; Li, Q.; Zhu, G. One-Pot Synthesis of Highly Ordered Nitrogen-Containing Mesoporous Carbon with Resorcinol-Urea-Formaldehyde Resin for CO_2 Capture. *Carbon* **2014**, *69*, 502–514. [CrossRef]
14. Creamer, A.E.; Gao, B. Carbon-Based Adsorbents for Postcombustion CO_2 Capture: A Critical Review. *Environ. Sci. Technol.* **2016**, *50*, 7276–7289. [CrossRef] [PubMed]
15. Wang, S.; Li, W.; Zhang, L.; Jin, Z.; Lu, A.-H. Polybenzoxazine-Based Monodisperse Carbon Spheres with Low-Thermal Shrinkage and Their CO_2 Adsorption Property. *J. Mater. Chem. C* **2015**, *3*, 4406–4412. [CrossRef]
16. Singh, G.; Lakhi, K.S.; Sil, S.; Bhosale, S.V.; Kim, I.Y.; Albahily, K.; Vinu, A. Biomass Derived Porous Carbon for CO_2 Capture. *Carbon* **2019**, *148*, 164–186. [CrossRef]
17. Alhwaige, A.A.; Ishida, H.; Qutubuddin, S. Carbon Aerogels with Excellent CO_2 Adsorption Capacity Synthesized from Clay-Reinforced Biobased Chitosan-Polybenzoxazine Nanocomposites. *ACS Sustain. Chem. Eng.* **2016**, *4*, 1286–1295. [CrossRef]
18. Liu, J.; Chen, C.; Zhang, K.; Zhang, L. Applications of Metal–Organic Framework Composites in CO_2 Capture and Conversion. *Chin. Chem. Lett.* **2021**, *32*, 649–659. [CrossRef]
19. Mohamed, M.G.; Samy, M.M.; Mansoure, T.H.; Li, C.J.; Li, W.C.; Chen, J.H.; Zhang, K.; Kuo, S.W. Microporous Carbon and Carbon/Metal Composite Materials Derived from Bio-Benzoxazine-Linked Precursor for CO_2 Capture and Energy Storage Applications. *Int. J. Mol. Sci.* **2022**, *23*, 347. [CrossRef]
20. Samy, M.M.; Mohamed, M.G.; Kuo, S.W. Directly Synthesized Nitrogen-and-Oxygen–Doped Microporous Carbons Derived from a Bio-Derived Polybenzoxazine Exhibiting High-Performance Supercapacitance and CO_2 Uptake. *Eur. Polym. J.* **2020**, *138*, 109954. [CrossRef]
21. Wan, L.; Wang, J.; Sun, Y.; Feng, C.; Li, K. Polybenzoxazine-Based Nitrogen-Containing Porous Carbons for High-Performance Supercapacitor Electrodes and Carbon Dioxide Capture. *RSC Adv.* **2015**, *5*, 5331–5342. [CrossRef]

22. Konnola, R.; Anirudhan, T.S. Efficient Carbon Dioxide Capture by Nitrogen and Sulfur Dual-Doped Mesoporous Carbon Spheres from Polybenzoxazines Synthesized by a Simple Strategy. *J. Environ. Chem. Eng.* **2020**, *8*, 103614. [CrossRef]
23. Bucior, B.J.; Chen, D.L.; Liu, J.; Johnson, J.K. Porous Carbon Nanotube Membranes for Separation of H_2/CH_4 and CO_2/CH_4 Mixtures. *J. Phys. Chem. C* **2012**, *116*, 25904–25910. [CrossRef]
24. Kyotani, T. Control of Pore Structure in Carbon. *Carbon* **2000**, *38*, 269–286. [CrossRef]
25. Rodríguez-Reinoso, F.; Sepúlveda-Escribano, A. Porous Carbons in Adsorption and Catalysis. *Handb. Surf. Interfaces Mater.* **2001**, *5*, 309–355. [CrossRef]
26. Manocha, S. Porous Carbon. In *Carbon. Alloy, Novel Concepts to Develop Carbon. Science and Technology*; Elsevier: Amsterdam, The Netherlands, 2003; Volume 28, pp. 335–348. [CrossRef]
27. Xia, Y.; Mokaya, R.; Walker, G.S.; Zhu, Y. Superior CO_2 Adsorption Capacity on N-Doped, High-Surface-Area, Microporous Carbons Templated from Zeolite. *Adv. Energy Mater.* **2011**, *1*, 678–683. [CrossRef]
28. Jin, Z.E.; Wang, J.L.; Zhao, R.J.; Guan, T.T.; Zhang, D.D.; Li, K.X. Synthesis of S, N Co-Doped Porous Carbons from Polybenzoxazine for CO_2 Capture. *New Carbon Mater.* **2018**, *33*, 392–401. [CrossRef]
29. Hao, G.P.; Li, W.C.; Qian, D.; Wang, G.H.; Zhang, W.P.; Zhang, T.; Wang, A.Q.; Schüth, F.; Bongard, H.J.; Lu, A.H. Structurally Designed Synthesis of Mechanically Stable Poly(Benzoxazine-Co-Resol)-Based Porous Carbon Monoliths and Their Application as High-Performance CO_2 Capture Sorbents. *J. Am. Chem. Soc.* **2011**, *133*, 11378–11388. [CrossRef]
30. Hong, L.; Ju, S.; Liu, X.; Zhuang, Q.; Zhan, G.; Yu, X. Highly Selective CO_2 Uptake in Novel Fishnet-like Polybenzoxazine-Based Porous Carbon. *Energy Fuels* **2019**, *33*, 11454–11464. [CrossRef]
31. Sevilla, M.; Parra, J.B.; Fuertes, A.B. Assessment of the Role of Micropore Size and N-Doping in CO_2 Capture by Porous Carbons. *ACS Appl. Mater. Interfaces* **2013**, *5*, 6360–6368. [CrossRef]
32. Le, T.H.; Yoon, H. Strategies for Fabricating Versatile Carbon Nanomaterials from Polymer Precursors. *Carbon* **2019**, *152*, 796–817. [CrossRef]
33. Yang, Y.; Le, T.H.; Kang, F.; Inagaki, M. Polymer Blend Techniques for Designing Carbon Materials. *Carbon* **2017**, *111*, 546–568. [CrossRef]
34. Al Aiti, M.; Jehnichen, D.; Fischer, D.; Brünig, H.; Heinrich, G. On the Morphology and Structure Formation of Carbon Fibers from Polymer Precursor Systems. *Prog. Mater. Sci.* **2018**, *98*, 477–551. [CrossRef]
35. Tiwari, I.; Sharma, P.; Nebhani, L. Polybenzoxazine—An Enticing Precursor for Engineering Heteroatom-Doped Porous Carbon Materials with Applications beyond Energy, Environment and Catalysis. *Mater. Today Chem.* **2022**, *23*, 100734. [CrossRef]
36. Zhang, C.; Wang, R.; Wang, Y.; Ren, G.; Zhang, X.; Li, R.; Fan, C. Synthesis of Millimeter-Sized Porous Carbon Spheres Derived from Different Precursors for CO_2 Capture. *J. Porous Mater.* **2021**, *28*, 81–91. [CrossRef]
37. Cai, Q.; Huang, Z.H.; Kang, F.; Yang, J.B. Preparation of Activated Carbon Microspheres from Phenolic-Resin by Supercritical Water Activation. *Carbon* **2004**, *42*, 775–783. [CrossRef]
38. Liu, F.; Huang, K.; Wu, Q.; Dai, S. Solvent-Free Self-Assembly to the Synthesis of Nitrogen-Doped Ordered Mesoporous Polymers for Highly Selective Capture and Conversion of CO_2. *Adv. Mater.* **2017**, *29*, 1700445. [CrossRef] [PubMed]
39. Kwiatkowski, J.F. *Activated Carbon: Classifications, Properties and Applications*; Nova Science Publishers: New York, NY, USA, 2012; ISBN 9781620816660.
40. Molina-Sabio, M.; González, M.T.; Rodriguez-Reinoso, F.; Sepúlveda-Escribano, A. Effect of Steam and Carbon Dioxide Activation in the Micropore Size Distribution of Activated Carbon. *Carbon* **1996**, *34*, 505–509. [CrossRef]
41. Mohamed, A.R.; Mohammadi, M.; Darzi, G.N. Preparation of Carbon Molecular Sieve from Lignocellulosic Biomass: A Review. *Renew. Sustain. Energy Rev.* **2010**, *14*, 1591–1599. [CrossRef]
42. Tagutchou, J.P.; Van De Steene, L.; Escudero Sanz, F.J.; Salvador, S. Gasification of Wood Char in Single and Mixed Atmospheres of H_2O and CO_2. *Energy Sources Part. A Recover. Util. Environ. Eff.* **2013**, *35*, 1266–1276. [CrossRef]
43. Bansal, R.C.; Goyal, M. *Activated Carbon Adsorption*; Taylor & Francis: London, UK, 2005; ISBN 9780824753443.
44. Chattopadhyaya, G.; Macdonald, D.G.; Bakhshi, N.N.; Soltan Mohammadzadeh, J.S.; Dalai, A.K. Preparation and Characterization of Chars and Activated Carbons from Saskatchewan Lignite. *Fuel Process. Technol.* **2006**, *87*, 997–1006. [CrossRef]
45. Teng, H.; Wang, S.C. Preparation of Porous Carbons from Phenol-Formaldehyde Resins with Chemical and Physical Activation. *Carbon* **2000**, *38*, 817–824. [CrossRef]
46. Sahu, J.N.; Acharya, J.; Meikap, B.C. Optimization of Production Conditions for Activated Carbons from Tamarind Wood by Zinc Chloride Using Response Surface Methodology. *Bioresour. Technol.* **2010**, *101*, 1974–1982. [CrossRef] [PubMed]
47. Knop, A.; Pilato, L. *Phenolic Resins: Chemistry, Applications and Performance*; Springer: Berlin/Heidelberg, Germany, 1985; ISBN 2013206534.
48. Lu, G.Q.; Do, D.D. Structure Changes of Coal Reject Char during Pyrolysis at Low Heating Rates. *Fuel Process. Technol.* **1991**, *28*, 247–258. [CrossRef]
49. Byrne, C.E.; Nagle, D.C. Carbonization of Wood for Advanced Materials Applications. *Carbon* **1997**, *35*, 259–266. [CrossRef]
50. Cetin, E.; Moghtaderi, B.; Gupta, R.; Wall, T.F. Influence of Pyrolysis Conditions on the Structure and Gasification Reactivity of Biomass Chars. *Fuel* **2004**, *83*, 2139–2150. [CrossRef]
51. Tay, J.H.; Chen, X.G.; Jeyaseelan, S.; Graham, N. Optimising the Preparation of Activated Carbon from Digested Sewage Sludge and Coconut Husk. *Chemosphere* **2001**, *44*, 45–51. [CrossRef] [PubMed]

52. Lua, A.C.; Lau, F.Y.; Guo, J. Influence of Pyrolysis Conditions on Pore Development of Oil-Palm-Shell Activated Carbons. *J. Anal. Appl. Pyrolysis* **2006**, *76*, 96–102. [CrossRef]
53. Guo, Z.; Lu, X.; Xin, Z. N, S, O Co-Doped Porous Carbons Derived from Bio-Based Polybenzoxazine for Efficient CO_2 Capture. *Colloids Surf. A Physicochem. Eng. Asp.* **2022**, *646*, 128845. [CrossRef]
54. Bae, Y.S.; Snurr, R.Q. Development and Evaluation of Porous Materials for Carbon Dioxide Separation and Capture. *Angew. Chem.-Int. Ed.* **2011**, *50*, 11586–11596. [CrossRef]
55. Wang, Q.; Luo, J.; Zhong, Z.; Borgna, A. CO_2 Capture by Solid Adsorbents and Their Applications: Current Status and New Trends. *Energy Environ. Sci.* **2011**, *4*, 42–55. [CrossRef]